Controlling the Formation of Antimicrobial Peptide Films: Fully-Developed Helical Peptides Are Required to Obtain a Homogenous Coating over a Large Area

Marta De Zotti,[a] Gabriele Corvi,[b] Emanuela Gatto,[b] Benedetta Di Napoli,[b] Claudia Mazzuca,[b] Antonio Palleschi,[b] Ernesto Placidi,[c] Barbara Biondi,[d] Marco Crisma,[d] Fernando Formaggio,[a,d] Claudio Toniolo,[a,d] and Mariano Venanzi*,[b]

[a] Department of Chemistry, University of Padova, 35131 Padova, Italy

[b] Department of Chemical Science and Technologies, University of Rome Tor Vergata, 00133 Rome, Italy

[c] ISM Unit, CNR, Department of Physics, University of Rome Tor Vergata, 00133 Rome, Italy

[d] Institute of Biomolecular Chemistry, CNR, Padova Unit, Department of Chemistry, University of Padova, 35131 Padova, Italy

Abstract: The influence of conformational dynamics on the self-assembly process of a novel, conformationally constrained, analogue of the natural, antimicrobial peptide trichogin GA IV was analysed by spectroscopic methods, microscopy imaging at nanometric resolution, and molecular dynamics simulations. The formation of antimicrobial peptide films at the air/water interface and their deposition on a graphite or a mica substrate were investigated. Combining experimental evidence with molecular dynamics simulation, we demonstrate that only the fully-developed helical structure of the analogue promotes formation of ordered aggregates nucleating the growth of micrometric rods, that give rise to homogenous coating over wide regions of the hydrophilic mica. This work proves the influence of helix flexibility on peptide self-organization and orientation on surfaces, key steps in the interaction of antimicrobial peptides with their target biological membranes.

Introduction

Antimicrobial peptides (AMPs) have been gaining increasing interest in the scientific community engaged in the fight against antibiotic resistance.[1] Indeed, AMPs belonging to the innate immune system have been found to exert a broad-band action against pathogens interacting selectively with the lipid bilayer of bacterial membranes.[2] Unfortunately, natural AMPs suffer from several drawbacks. Relevant among them are short survival times and low targeting capability.[3]

An alternative approach to overcome these problems, in particular to minimize the immunogenic response, aims at developing bioactive peptide analogues based on non-coded amino acids.[4]

Peptaibols are a class of AMPs, from 5 to 20 residues long, characterized by the usually massive presence in their main chain of α-aminoisobutyric acid residues, a dimethyl $C^{\alpha,\alpha}$-substituted α-amino acid (denoted as Aib or U in the three- or single-letter code, respectively).[5]

Theoretical and experimental studies demonstrated that the dimethyl substitution at the C^{α} atom strongly restricts the allowed conformational space for Aib residues.[6] As a consequence, Aib-rich oligopeptides tend to attain ordered backbone conformations, with a characteristic switch between 3_{10}- and α-helical structures depending on the percentage of constituent Aib residues and the length of the main chain. The 3D-structural and self-assembly properties of this class of compounds have been recently reviewed by some of us.[7]

One of the most extensively investigated member of the peptaibol family is trichogin GA IV (**TrGA**), isolated in 1992 by Bodo and co-workers[8] and firstly synthesized in 1994 by Toniolo and co-workers.[9] **TrGA** is an N-acylated decapeptide hydroxyalkylamide, characterized by the sequence *n*Oct-Aib-Gly-Leu-Aib-Gly-Gly-Leu-Aib-Gly-Ile-Lol, where *n*Oct- stands for the *n*-octanoyl group and Lol for the C-terminal 1,2-aminoalcohol leucinol (Scheme 1). From a conformational point of view, the **TrGA** sequence is rather peculiar, featuring as many as four (out of ten) Gly residues (the most conformationally flexible among the 20 coded amino acids) counterbalanced by three constrained Aib residues. NMR and X-ray diffraction studies allowed to determine the 3D-structure of **TrGA** in methanol solution and in racemic crystals, respectively. This short-length peptaibol predominantly adopts a mixed 3_{10}-/α-helix structure, specifically a distorted 3_{10}-helix at the N-terminus and a longer α-helical segment at the C-terminus.[9] X-Ray diffraction data also revealed the amphiphilic character of **TrGA**, with the *n*-octanoyl moiety, and the Leu and Ile side chains forming the hydrophobic region of the helix, while the four Gly residues are positioned in the opposite region. Aib methyl groups align on the borderland.

The dynamic properties of some **TrGA** analogues were also studied in detail by time-resolved spectroscopy and theoretical conformational analysis, determining the kinetics of the conformational transition between a 2-nm long helical structure and a more compact conformation

characterized by a bend involving the central Gly-Gly residues.[10,11] Interestingly, it was shown that the population of the latter conformation is favoured by the association of bi- and trivalent metal ions, like Ca(II) and Gd(III).[12] More recently, we coated a gold platform with a thiolated **TrGA** analogue to anchor lipid bilayers into nanometric cavities.[13]

TrGA is a membrane-active peptide. The achievement of a critical **TrGA** concentration in the presence of liposomes promotes formation of transient pores, which involves enhanced dynamics of the phospholipid chains and leakage of the incorporated material from the inner region.[14] The mechanism of **TrGA** antimicrobial activity, ruled by a delicate balance between peptide aggregation in solution and in the membrane outer surface,[15,16] is not yet completely understood.

Aggregation studies of AMPs at the air-water interface by Langmuir-Blodgett (LB) techniques offered important insights on the mechanism of their antimicrobial activity.[17] LB peptide films showed a rich morphology, like 'butterfly shapes', rectangles, dots, nanofibers or nanoribbons. However their ability to self-organize into fibril-like nanostructures seems to be crucial for their bioactivity.[18,19] Very recently, some of us characterized by molecular dynamics (MD) simulations the behaviour of **TrGA** at the air/water interface during a LB compression.[20] It was shown that, on increasing the surface pressure, several structural changes take place: at first, globular aggregates coalesce giving rise to fibrillization. Then, nanofibers form a network in which meshes are filled by water pools. MD results also indicated that during those transitions the peptide chains are located almost parallel to the surface, adopting a predominantly helical conformation. At higher surface pressures, **TrGA** chains partially unfold, assuming a vertically-aligned arrangement with respect to the air/water interface. Such horizontal-to-vertical transition of helical peptide films has been already reported in the literature and well characterized by polarized infrared (IR) spectroscopy.[21,22] All of the abovementioned results strongly suggest that the 3D-structural and dynamic properties of the peptide chains deeply affect their self-assembly process, determining the morphology of the films and their overall organization at the air/water interface.

The major target of this work was to investigate the dependence of the LB film formation on the 3D-structural and dynamic properties of **TrGA**, by comparing its performance with that of an analogue designed to be much more conformationally restricted. To this aim, the first eight amino acid residues of the parent peptide chain were significantly modified, in particular by replacing its three Gly residues with helicogenic Leu residues. Moreover, the additional Gly residue near the C-terminus was suppressed (Scheme 1). These substitutions removed all of the conformationally flexible residues from the **TrGA** main chain, severely reducing the allowed Ramachandran φ,ψ space of the analogue, denoted in the following as **TrGAr** to emphasize its restricted dynamics.

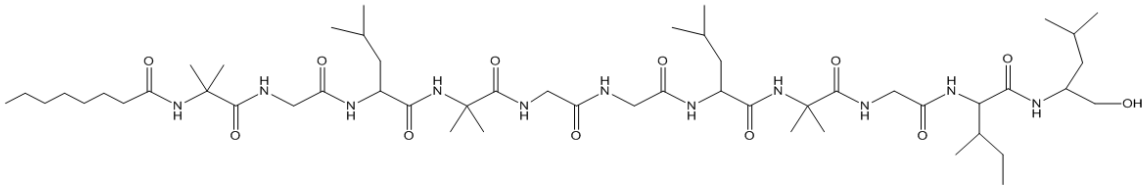

***n*Oct-Aib-Gly-Leu-Aib-Gly-Gly-Leu-Aib-Gly-Ile-Lol (TrGA)**

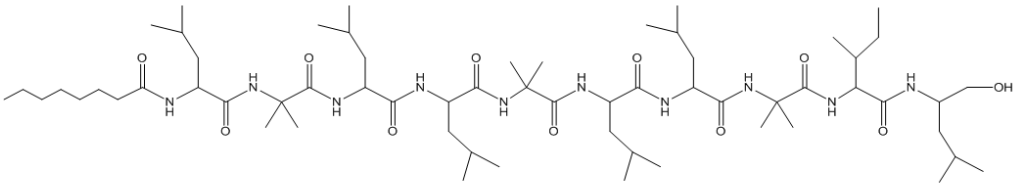

***n*Oct-Leu-Aib-Leu-Leu-Aib-Leu-Leu-Aib-Ile-Lol (TrGAr)**

Scheme 1. Molecular formulas and acronyms for trichogin GA IV (**TrGA**) and its conformationally constrained analogue (**TrGAr**).

Results

Conformational analysis

As a first step, we performed a thorough 3D-structural analysis both in solution (by CD and NMR, see *Supporting Information*, *§SI3.1* and *§SI3.2*, respectively) and in the crystal state (by X-ray diffraction, see *§SI3.3* and below) of the newly synthesized **TrGAr** analogue, comparing its conformational preferences with those of natural **TrGA**.

CD experiments in methanol and methanol/water (70/30 *v*/*v*) solutions, highlighted that in both environments **TrGA** attained the typical CD spectrum of a mixed 3_{10}-/α-helix, characterized by a ratio (R)[23] between the signal intensities at 222 and 208 nm ($[\theta]_{222}/[\theta]_{208}$) of 0.4 (Figure S4A, *§SI3.1*)[24]. The structure-stabilizing effects of the sequence modification in **TrGAr** are clearly revealed by its CD spectrum in methanol and, more notably, in the methanol/water (70/30, *v*/*v*) solution where the peptide hydrophobicity favours self-aggregation. The CD spectrum in the latter environment is that of a canonical α-helix, but with R>1, indicating that the regular α-helical structures of **TrGAr** self-assemble in the presence of water, supported by hydrophobic effects (Figure SI4B, *§SI3.1*).

We acquired 2D-NMR spectra of **TrGAr** in deuterated methanol. A detailed description and two portions of the ROESY[25] spectrum are reported in the *Supporting Information (§SI2.2)*. The ROESY *fingerprint* region shows long-range connectivities diagnostic of a 3_{10}-helix. Taken together, the results of CD and 2D NMR analysis in solution confirms the onset of a well-developed helical conformation throughout the sequence of **TrGAr**, with a higher percentage of 3_{10}-helical structure in methanol.

The molecular structure of **TrGAr**, as determined by single crystal X-ray diffraction analysis, is illustrated in Figure 1. Relevant (backbone and side-chain) torsion angles and H-bond parameters are reported in the *Supporting Information* (Tables SI2 and SI3, respectively). The peptide is folded in a α-helical conformation stabilized by nine intramolecular C=O···H-N H-bonds. Specifically, starting from the N-terminus, the *n*Oct C=O group is the acceptor of two H-bonds, from the N-H groups of Leu(3) and Leu(4), thus giving rise to a β-turn (C_{10} form) encompassed within an α-turn (C_{13} form).[26] Then, six consecutive C=O···H-N intramolecular H-bonds of the α-turn-type are observed. The helix terminates with an oxy-analogue of an α-turn,[27] the H-bond donor of which is the hydroxyl group of the C-terminal Lol and the Leu(7) carbonyl oxygen is the acceptor. The backbone ϕ,ψ torsion angles, as averaged over residues 1-9, are -63.3° and -44.1°, very close to the canonical values (-63°, -42°) based on statistical analysis of α-helices in crystalline peptides.[28] The ϕ,"ψ" (the latter torsion angle referring to the N10-C10A-C10-O10 atom sequence) values adopted by the C-terminal Lol are -128.1°, 63.2°. The regularity of the α-helix and the quite even distribution of the hydrophobic side chains along the helical envelope stand out clearly from the projection of the molecule as viewed along the helix axis (Figure 1B).

In the packing mode, two intermolecular H-bonds are seen, connecting the N-H groups of Leu(1) and Aib(2), respectively, to the C=O groups of Aib(8) and Ile(9) of a (x+1, y, z+1) symmetry related molecule. As a result, head-to-tail H-bonded rows of molecules are generated along the *ac* direction. Lateral packing among helical rows is then achieved through van der Waals interactions involving *n*Oct and aliphatic side chains (Figure SI7, *§SI2.3*), as commonly observed for apolar helical peptides.[29]

In summary, our conformational analysis demonstrated that **TrGAr** adopts a fully-developed helical 3D-structure under all investigated experimental conditions. Both CD and 2D NMR evidenced that a 3_{10}-helix is preferentially adopted by **TrGAr** in the structure-supporting solvent methanol, while a α-helical conformation is largely preferred in the crystal state and under conditions favouring self-aggregation, *e.g.*, in the presence of water. The conformational preferences of the natural **TrGA** has already been reported in the literature under a variety of experimental conditions. In contrast with **TrGAr**, the natural antimicrobial peptide adopts a flexible, mixed 3_{10}-/α-helical 3D-structure both in solution and in the crystal state.[9]

A

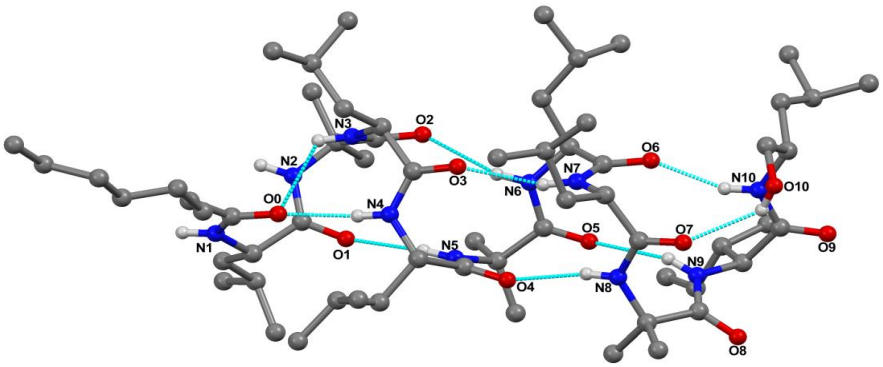

B

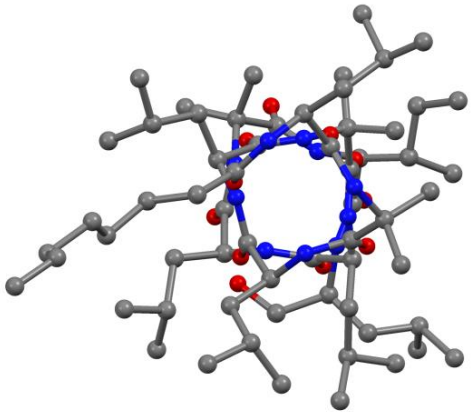

Figure 1. X-Ray diffraction structure of **TrGAr** as viewed (**A**) perpendicularly and (**B**) along the helix axis. Most of the H-atoms are omitted for clarity. In **A**, intramolecular H-bonds are indicated by dashed lines.

Langmuir-Blodgett peptide films

In the well-established LB technique few hundred microliters of a volatile, water-insoluble micromolar solution of an amphiphilic molecule is spread on an aqueous sub-phase. After evaporation of the volatile solvent, a very thin organic film forms at the air/water interface. The packing and morphology of the film can be suitably varied, closing the mobile barriers of the LB trough. At high surface pressures, the organic film may eventually collapse in a so-called solid phase, characterized by formation of 3D-aggregates. The organic monolayer can be easily deposited on a solid substrate at a selected surface pressure, and the thickness of the organic film can be varied by repeated immersion/emersion cycles. The entire process is controlled by recording surface pressure (Π) *versus* Mma isotherms during the closing of the mobile barriers.

Interesting differences in the process of film formation at the air/water interface between the two peptides were revealed by the Π *versus* Mma curves, reported in Figures 2A and 2B for **TrGA** and **TrGAr**, respectively. Figure 2A shows that the **TrGA** compression is characterised by a continuous increase of the surface pressure in the region from 400 to 100 Å^2/molecule until the collapse of the LB isotherm at around 37 mN/m. This inflection point clearly indicates a drastic change of the morphology of the peptide film (3D-collapse).

It should be considered that the molecular area occupied at the air/water interface by a single **TrGA** molecule in a helical conformation is about 185 Å^2 for a disposition of the peptide chain parallel to the aqueous surface and about 80 Å^2 for a perpendicular arrangement. As a consequence, Mma areas below 150 Å^2/molecule can be explained only by a structural rearrangement of the peptide film, *i.e.* a transition from a parallel to a vertical arrangement of the helices, increasing the thickness of the peptide monolayer. Very low Mma values, *i.e.* below 60 Å^2/molecule, can be associated with formation of 3D-nanostructures and thick peptide multilayers.

Interestingly, the **TrGAr** isotherm presents the typical feature of a first-order transition curve, characterised by a constant surface pressure (Π ≈20 mN/m) extending in the Mma region comprised between 250 and 100 Å^2/molecule (Figure 2B). At higher surface pressures, a steep rise of the isotherm is seen, but no collapse of the curve could be found at the maximum surface pressure investigated (Π ≈27 mN/m), corresponding to Mma≈50 Å^2/molecule.

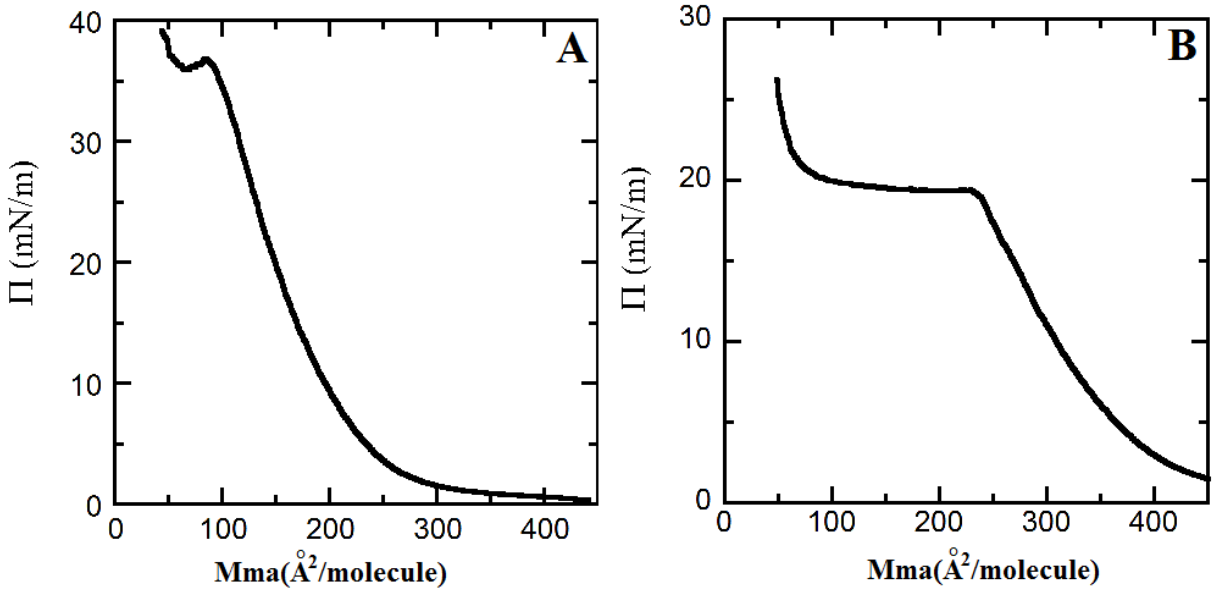

Figure 2. Surface pressure Π *versus* Mma isotherms for **TrGA** (**A**) and **TrGAr** (**B**).

Cyclically repeated Π *versus* Mma isotherms showed a marked hysteresis for both **TrGA** and **TrGAr** LB curves, suggesting the onset of aggregates at the air/water interface.[30] Nonetheless, the

first order-like character of the **TrGAr** isotherm is maintained for all of the repeated compression/expansion cycles (Figure SI8, *§SI4.2*).

The different aggregation properties at the air/water interface of **TrGA** and **TrGAr** are further highlighted by considering the variation of the compressibility modulus of the two peptide films under increasing surface pressure conditions (Figure 3). The compressibility modulus *K* is defined as:

$$K = -A\left(\frac{d\Pi}{dA}\right)_T$$

where *A* is Mma. Basically, the higher the value of *K*, the tighter is the lateral packing of the molecules.[31]

Interestingly, from Figure 3A it can be seen that the compressibility modulus of **TrGA** steadily increases from Mma=350 Å^2/molecule, reaching a maximum at about 130 Å^2/molecule. At lower Mma values the compressibility modulus markedly decreases. The fall-off of *K*, associated to the collapse of the LB isotherm at high surface pressures (Figure 2A), suggests that this effect is caused by formation of peptide 3D-aggregates, which produces a marked decrease of Mma without increasing the surface pressure. It was argued[20] that such transition is associated to a partial loss of the helical conformation, allowing for a more compact arrangement of the peptide chains.

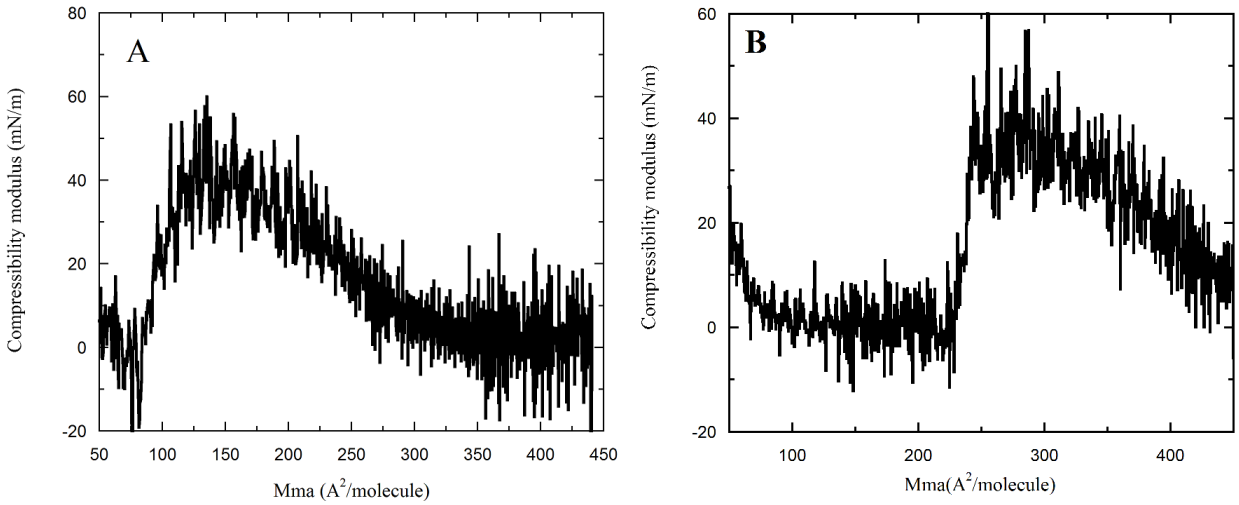

Figure 3. Compressibility modulus *versus* Mma for **TrGA** (**A**) and **TrGAr** (**B**).

In the case of **TrGAr**, after an initial increase of the compressibility modulus at large Mma values, a region of almost null *K*, associated with the flat region of the LB isotherm (Figure 2B), indicates the occurrence of a *quasi*-reversible transition, characterised by a marked reduction in Mma without an increase in the compressibility factor. We associate the region of low compressibility factors extending from Mma ~250 to ~100 Å^2/molecule to a horizontal-to-vertical rearrangement of the

TrGAr helices. The corresponding compressibility factors begin to increase only when this transition is completed (Mma≈75 Å^2/molecule).

It is also instructive to consider the deposition processes of **TrGA** and **TrGAr** on hydrophobic (graphite) and hydrophilic (mica) substrates, as quantified by the transfer ratio (t.r.) coefficient, *i.e.* the ratio between the decrease in the monolayer area during a deposition stroke and the area of the substrate (Table SI4, *§SI4.2*). Interestingly, while **TrGA** shows positive t.r. values regardless of the nature of the substrate, **TrGAr** exhibits preferential deposition only on hydrophilic mica. For both compounds, deposition at high surface pressures gives rise to t.r. values well above the ideal unit, suggesting deposition of aggregated species on the substrates.

To shed light on the rationale at the molecular level behind the differences observed for the two peptides in the formation of the LB films, MD simulations were carried out for **TrGAr** at a number density of 16, 28 and 60 peptide molecules/Å^2, corresponding to a mean molecular area of 450, 260 and 130 Å^2 /molecule, respectively. The recently published results of MD simulations on **TrGA**[20] are here reported for comparison.

From the data collected in Table 1, it is clear that **TrGA** experiences a marked increase in unordered structures, *i.e.* turn/coil structures, as the peptide number density at the air/water interface increases. Conversely, **TrGAr** maintains a significant content of helical structures even at the high density of 60 molecules/Å^2, corresponding to Mma=130 Å^2 /molecule.

Table 1. Percentage of secondary structure of **TrGA** and its conformationally-constrained analogue **TrGAr** from MD simulations

	TrGA		**TrGAr**	
Area (Å^2/molecule)	% helix	% turn/coil	% helix	% turn/coil
450	69.6	31.4	69.0	31.0
260	60.2	39.8	67.7	32.3
130	15.5	84.5	42.0	58.0

Figure 4A shows that both **TrGA** and **TrGAr** at low density (Mma=450 Å^2 /molecule) form small aggregates, organized in nanometric domains stabilised by interhelical interactions. Besides, only **TrGAr** molecules tend to align in a regular head-to-tail arrangement even at such low density. A similar behaviour is not observed for **TrGA** molecules. At 270 Å^2 /molecule (Figure 4B), both **TrGA** and **TrGAr** give rise to an ordered 2D-network, enclosing small water pools. However, the

TrGAr grid appears more tightly fitted than the loosely entangled **TrGA** chains, most likely because of more extended interhelical interactions in the former case.

At 130 Å^2 /molecule the helical content of **TrGA** markedly decreases, in favour of turn/coil conformations. Self-assembly of those unordered structures leads to a densely packed arrangement, the morphology of which is mainly determined by hydrophobic effects. On the contrary, **TrGAr** maintains a predominantly helical 3D-structure (Figure 4C), that can stabilise the peptide film through inter-helical interactions. Indeed, the long-lasting surface pressure plateau in the **TrGAr** isotherm from Mma 250 to 100 Å^2 /molecule points to the occurrence of a *quasi*-reversible transition associated to the formation of a thick peptide layer stabilised by attractive (van der Waals) inter-helical interactions. The side views of the **TrGA** and **TrGAr** films at the air/water interface reported in Figure 4D, clearly demonstrate the influence of the helical content on the different morphologies attained by the two peptide layers.

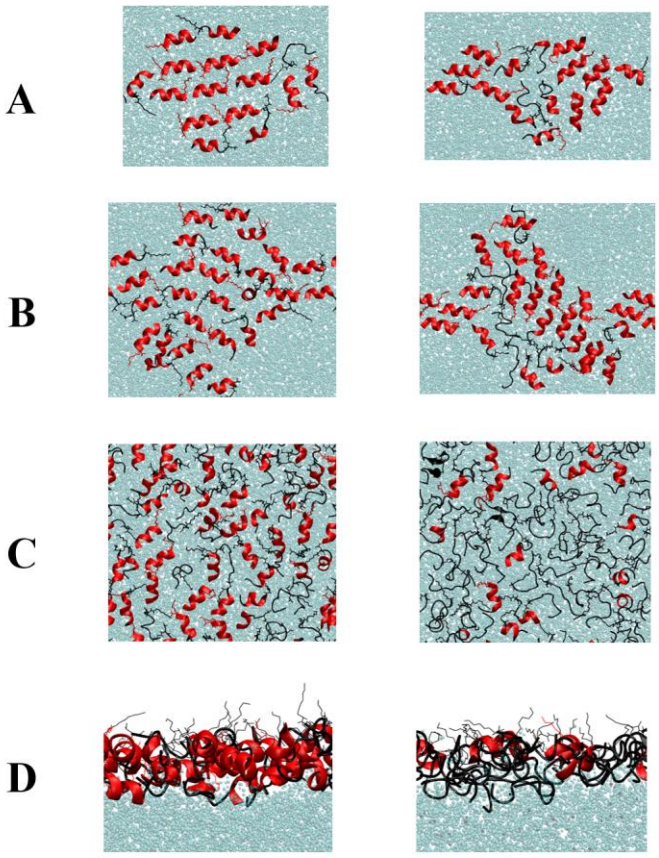

Figure 4. MD simulations of **TrGAr** (left column) and **TrGA** (right column). **A**: 16 peptide molecules in the unit cell (Mma=450 Å^2/molecule); **B**: 28 peptide molecules (Mma=260 Å^2/molecule); **C**: 60 peptide molecules (Mma=130 Å^2/molecule). **D**: Side views of **C**.

CD and FTIR-ATR spectroscopies in films

To experimentally confirm the MD data, we characterized the secondary structure of the two peptides **TrGA** and **TrGAr** in their LB films deposited on quartz by CD and FTIR-ATR spectroscopies.

The data reported in Figure 5A demonstrate that **TrGA** maintains in the film the same, mixed-type, helical 3D-structure populated in solution (*R*=0.5) under both surface pressures applied for LB deposition. Conversely, CD measurements on **TrGAr** LB films (Figure 5B) suggest a partial conformational transition as the surface pressure for LB deposition increases from 17 to 20 mN/m.

The measured *R* values (0.8 at Π=17 mN/m and 0.5 at Π=20 mN/m) indicate that at high surface pressures a partial α- to 3_{10}-helix transition does take place. It should be considered that the area projected by perpendicularly aligned **TrGAr** molecules in α-helix conformation is about 130 $Å^2$, to be compared with 80 $Å^2$ for the 3_{10}-helical **TrGAr**. This result suggests that the α- to 3_{10}-helix conversion can indeed occur together with the morphological transition suggested above from a horizontally layered peptide film to a predominantly vertical arrangement of the **TrGAr** main chains.

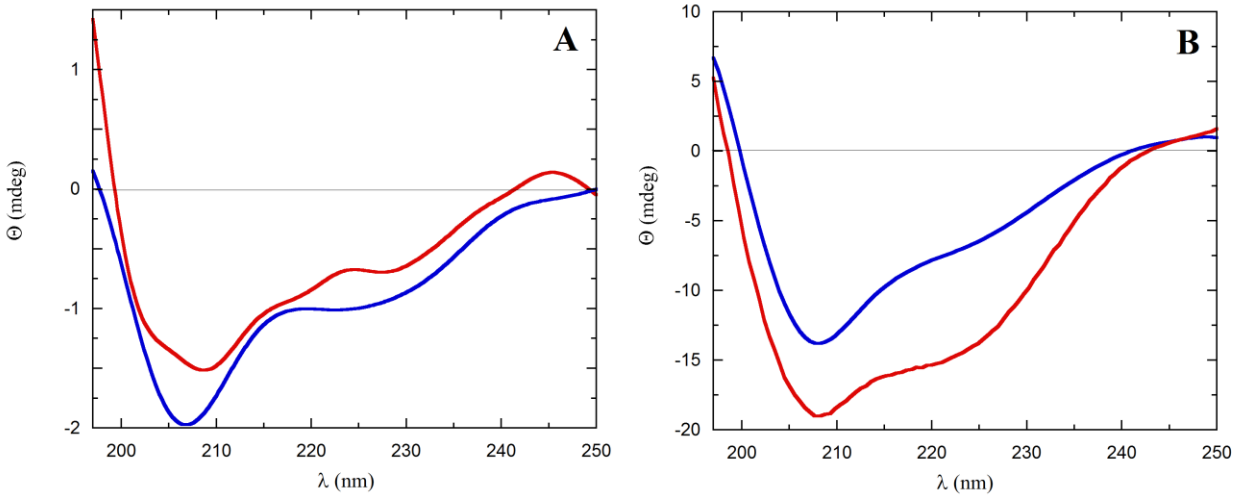

Figure 5. CD spectra of peptide films deposited on hydrophobic quartz. **A**: **TrGA**, red (Π=35 mN/m), blue (Π=39 mN/m); **B**: **TrGAr**, red (Π=17 mN/m), blue (Π=20 mN/m).

In agreement with the CD results, the deconvolution of the amide I band of the FTIR absorption spectra in the ATR mode demonstrates that **TrGA** in the LB film almost equally populates multiple conformations (β-turn, 3_{10}- and α-helices) with an additional significant presence of unordered (random coil) structures.[32] For the **TrGAr** film, unordered conformations are definitely of minor significance, with a predominant percentage of turn/helical structures (Table 2 and Figure SI9, *§SI4.3*).

Table 2. Amide I region of the FTIR-ATR spectra of **TrGA** and **TrGAr** LB films deposited on quartz at high surface pressures

Sample		TrGA	TrGAr
band maximum (cm^{-1})	secondary structure	relative intensity (%)	relative intensity (%)
~1630	β-turn	27	39
~1650	α-helix	28	21
~1666	3_{10}-helix	19	36
~1680	coil	26	4

Our CD and FTIR-ATR analyses suggest that at high surface pressures **TrGA** mainly populates unfolded and mixed-type helical conformations, and confirm the restricted conformational landscape and dynamics of the rigidified trichogin analogue.

Atomic force microscopy

AFM experiments were carried out on both **TrGA** and **TrGAr** films deposited on either a hydrophobic (HOPG) or a hydrophilic (mica) surface to analyse the influence of the substrate on their morphologies.

AFM images of the **TrGA** films deposited on graphite at surface pressures slightly below (35 mN/m) or above (39 mN/m), the high-pressure transition point, are reported in Figure 6. It is evident that **TrGA** gives films of similar morphology on both substrates. At the lowest investigated surface pressure, globular structures with heights ranging from 2 to 3.5 nm largely predominate on both substrates. At the higher surface pressure (*i.e.*, Π=39 mN/m), the film appears to self-organize in a dense layer, likely generated by collapsing of the globular structures, with an average height of 1.5 (±0.1) nm.

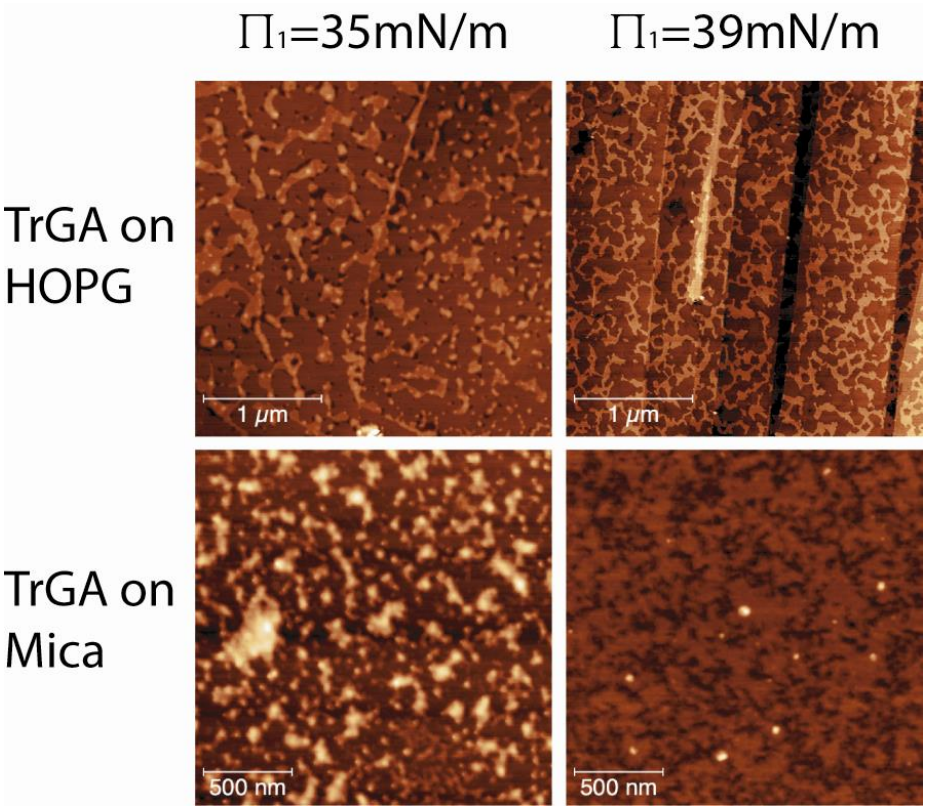

Figure 6. AFM topographies of **TrGA** LB films on graphite (HOPG, top row) and mica (bottom row).

A reduction of the average roughness from 1.14 to 0.18 nm and from 0.75 to 0.65 nm on both mica and HOPG substrates, respectively, was observed by increasing the surface pressure conditions used for deposition. Interestingly, in limited regions of the peptide film on graphite and only at the highest investigated surface pressure, some rod-like nanometric structures were also detected (Figure SI10, *§SI4.3*).

For comparison, AFM images of **TrGAr** LB films on the graphite and mica substrates are reported in Figure 7. On the hydrophobic surface (top row), only small globular structures could be imaged regardless of the surface pressure. For deposition of the LB film at Π=17 mN/m, the average diameter and height of the globular aggregates imaged are 280 (±70) and 6.1 (±0.3) nm, respectively. At the highest investigated surface pressure, the globular structures are smaller and more dense, showing heights varying from 2.3 nm to 4.2 nm. Accordingly, also the average roughness of the peptide layer decreases from 1.61 (at Π=17 mN/m) to 0.61 nm (at Π=20 mN/m).

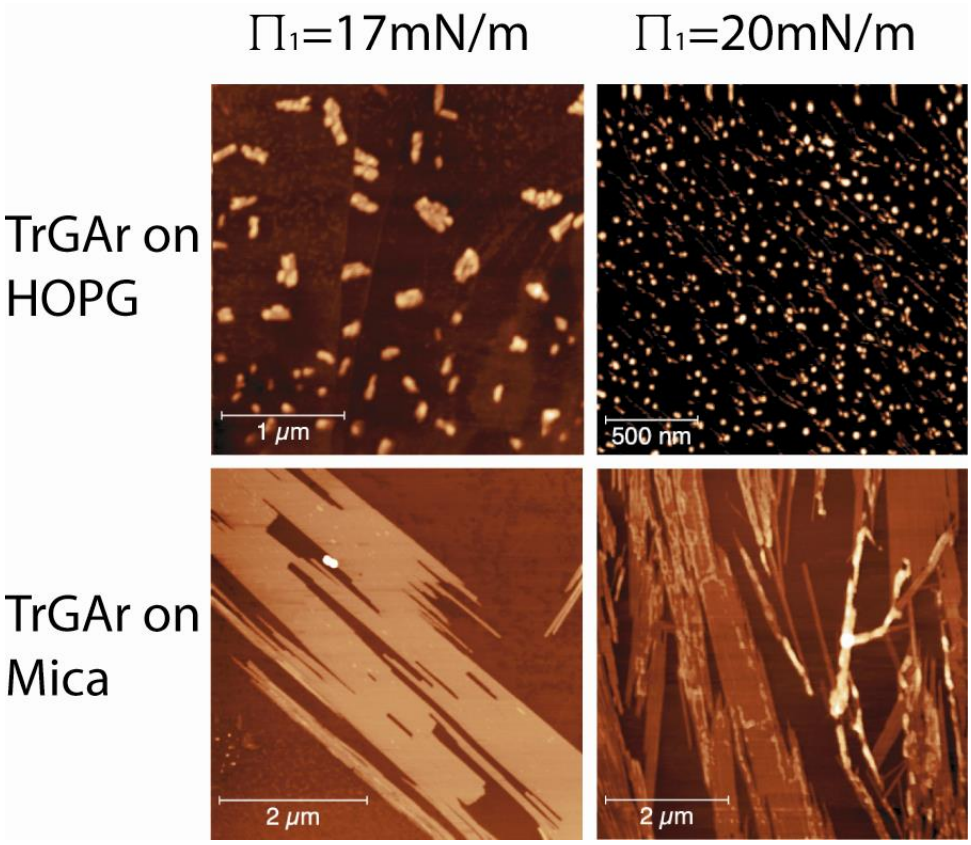

Figure 7. AFM topographies of **TrGAr** LB films on graphite (HOPG, top row) and mica (bottom row).

TrGAr LB films on mica showed a completely different morphology (Figure 7, bottom row). On this hydrophilic surface, an ordered arrangement of peptide rods of nanometric width and height [300 (±100) nm and 2.6 (±0.6) nm, respectively] and micrometric length [7(±2) μm] was imaged by AFM measurements, regardless of the surface pressure applied for depositing the peptide film.
At the higher surface pressure, these rods organise in large terraces, most likely produced by the LB compression of the peptide rods, that appear to be oriented perpendicularly to the direction of the closing barriers. Notably, in this case, the average roughness increases from 1.18 to 1.76 nm with increasing surface pressure.

Discussion

To analyze the effects of the removal and replacement of flexible Gly residues (in **TrGA**) with the helicogenic Aib and Leu residues (in **TrGAr**), three structural levels should be taken into account: (i) the secondary structure attained by the single peptide building block, (ii) the self-assembly of the peptide chains in small aggregates, and (iii) the formation of peptide films coating extended regions

of the solid substrates. In other words, a hierarchical process of peptide self-assembly from nano- to the mesoscopic scale should be followed.

At the level of the peptide secondary structure, **TrGAr** adopts a significantly restricted and well-developed helical structure both in solution and in the crystal state. CD and FTIR absorption data indicate that it has a remarkable propensity to populate helical conformations also when deposited on surfaces, with only a minor contribution from unordered (turn/coil) conformations. Clearly, the hindered dynamics of **TrGAr** limit its interconversion between the two (restricted) helical regions of the allowed low-energy conformers, as confirmed by MD simulations.

As for the self-assembly process leading to small aggregates nucleating the growth of micrometric structures, very recently we carried out MD simulation studies on the aggregation of **TrGA** at the air/water interface varying the peptide concentration on the aqueous surface.[20] We found that for a number of peptide molecules comprised between n=2 and 8 (corresponding to a Mma per peptide between 2500 and 950 $Å^2$/molecule) **TrGA** forms small drops based on its mixed helical conformation arranged parallel to the surface. Interestingly, aggregation and population of helical structures seem to be correlated (the cooperativity level of this process is currently under investigation).

For n=16-20 (Mma: 500-400 $Å^2$/molecule), **TrGA** peptide drops coalesce into nanofibers. Here **TrGA** molecules, still preferentially adopting a helical conformation, lay parallel to the aqueous surface. In the range $28 \leq n \leq 48$ (250-150 $Å^2$/molecule), the nanofibers interconnect and generate peptide networks embedding water pools (the water content is about 50%). At $n > 48$ (Mma < 150 $Å^2$/molecule) the meshes shrink abruptly (with a water content less than 15%), and the peptide forms a dense monolayer with the backbones vertically aligned with respect to the water surface.

Our AFM measurements confirmed those findings, revealing the formation of a dense network of peptide nanofibers which enclose smaller regions of entrapped water molecules. In the self-assembly of **TrGA**, hydrophobic effects predominate over the 3D-structuring effects. Globular structures are observed independently of the hydrophobic or hydrophilic nature of the substrate and of the surface pressure applied for LB deposition.[33,34]

Concerning the **TrGAr** analogue, the propensity of helical structures to promote formation of ordered layers is unambiguously demonstrated by the self-assembly process at the air/water interface monitored by the Π *versus* Mma LB isotherm and illustrated by MD simulations. AFM measurements strongly suggest that, in this case, the nature of the substrate plays an important role in determining the morphology of the peptide film. Only on the hydrophilic mica (but not on the hydrophobic HOPG), **TrGAr** forms micrometric rods, assembled in micrometric tapes at high surface pressure, coating homogeneously extended region of the solid substrate.

Conclusions

A synthetic, conformationally-constrained analogue (**TrGAr**) of the naturally-occurring antimicrobial peptide **TrGA** was obtained by substituting all flexible Gly residues with helicogenic Aib and Leu residues. The onset of a remarkably well-developed helical structure for **TrGAr** was confirmed by 2D-NMR and X-ray diffraction analysis. The effect of **TrGAr** enhanced conformational restrictions on the self-assembly properties of the natural **TrGA** was investigated by studying LB peptide films at the air/water interface. The differences in helical stability between the native **TrGA** sequence and **TrGAr** translated into significant changes in their aggregation processes, as indicated by the Π *versus* Mma LB isotherms, MD simulations, CD and FTIR-ATR absorption spectroscopies, and AFM imaging of peptide films on hydrophobic (HOPG) and hydrophilic (mica) surfaces. While **TrGA** forms only globular structures independently of the nature of the solid support, **TrGAr** promotes formation of extended flat regions on mica, as the result of the coalescence of micrometric rods. Our results clearly reveal the hierarchical nature of peptide self-assembly, that propagates the different properties of the single peptide building blocks to the mesoscopic scale of films coating extended regions of inorganic substrates.

Experimental Section

Synthesis and characterization. TrGA was synthesized as previously described.[35] **TrGAr** was produced by solid-phase peptide synthesis following a similar protocol, and fully characterized by ^{1}H NMR, ^{13}C NMR and ESI-HRMS (see *Supporting Information, §SI1*). Information on materials and spectroscopic (UV-Vis, CD, FTIR) techniques are detailed in *Supporting Information* (*§SI2*).

Conformational studies. The conformational preferences of the trichogin analogue **TrGAr** were assessed both in solution, by means of 2D-NMR (ROESY, TOCSY) and CD, and in the crystal state by solving its X-ray diffraction crystal structure. Details on 2D-NMR and X-Ray diffraction studies are provided in *Supporting Information* (*§SI3*). Relevant crystal data and structure refinement parameters are listed in Table S1 (*§SI3.3*). CCDC 1901624 contains the supplementary crystallographic data for this paper. They can be obtained free of charge from The Cambridge Crystallographic Data Centre via www.ccdc.cam.ac.uk/structures.

Langmuir-Blodgett experiments. Measurements of surface pressure (Π) *versus* mean molecular area (Mma) isotherms and deposition of multilayer films were carried out using a computer-controlled KSV LB (KSV MiniMicro, Helsinki, Finland) apparatus. Details on LB film preparation and deposition on hydrophobic (graphite, quartz) and hydrophilic (mica) substrates are given in *Supplementary Information* (*§SI4*). The surface pressure Π at each Mma was obtained from

Π(Mma)= γ_w - γ(Mma), where γ_w is the surface tension of water at 20°C and γ(Mma) is the surface tension of the system at Mma.

Atomic Force Microscopy. AFM measurements were performed in air by use of a Veeco Multiprobe IIIa (Veeco, Santa Barbara, CA) instrument. **TrGA** and **TrGAr** monolayers were deposited by the LB method on graphite (HOPG, hydrophobic) and on mica (hydrophilic), previously washed with Milli-Q water and ethanol, and then dried with a flux of argon at a fixed surface pressure. Experiments were carried out at room temperature (20°C) in the tapping mode (frequency=300 kHz) using SiO_2 Nanosensor tips with a spring constant of 42 N/m and a typical tip curvature radius of 7 nm.

Molecular dynamics simulations. The Gromacs 4.6.7[36] software with the GROMOS 53a6 force field[37] was used to perform MD simulations at a constant pressure and in a temperature ensemble (NPT) applying periodic boundaries conditions. Peptides were placed in the simulation box (9x9x27 nm^3) as two symmetrical monolayers, separated by a water slab (Single Point Charge model) of 3-nm thickness to eliminate interactions between the two monolayers. In the starting configuration, an α-helical conformation was adopted by each peptide with the helical axis perpendicular to the water surface. After energy minimization, the solvent was equilibrated using a 150 ps MD at 50 K, while the position of peptide molecules was restrained. The systems were gradually heated to 300 K through a 1-ns MD simulation and finally a 100 ns-long production run was performed (three replicas for each system). A cut-off of 1.4 nm for the electrostatic (PME algorithm) and the van der Waals interactions was selected, and temperature and pressure with semi-isotropic conditions were controlled by the Berendsen algorithm.[38] Topologies for all of the amino acids have been already reported.[20] All simulation analyses were performed during the last 10 ns of simulation time. The secondary structures were analysed using the DSSP (Define Secondary Structures of Proteins) GROMACS tool and visualized with the VMD software.[39]

Supporting Information

TrGA synthesis and characterization (*§SI1*, Figures SI1-SI3). Materials and spectroscopic techniques (*§SI2*). CD spectra of **TrGA** and **TrGAr** in methanol and (70/30 *v*/*v*) methanol/water solutions (*§SI3.1*, Figure SI4). 2D NMR of **TrGAr** in methanol solution (*§SI3.2*, Figures SI5 and SI6). X-Ray diffraction analysis (*§SI3.3*): crystal data and structure refinement (Table SI1); selected torsion angles (Table SI2); intra- and intermolecular hydrogen bond parameters (Table SI3); crystal packing of **TrGAr** as viewed along the ac direction (Figure SI7). LB films (*§SI4*): cyclic LB Π *versus* Mma isotherms (Figure SI8); transfer ratio coefficients for LB deposition (Table SI4); FTIR-

ATR spectra of **TrGA** and **TrGAr** on quartz (Figure SI9); AFM imaging of **TrGA** on graphite (Figure SI10).

Acknowledgements

This project has received funding from the European Union's Horizon 2020 Research and Innovation programme under the Marie Sklodowska-Curie grant agreement No. 690901. MDZ acknowledges MIUR (Futuro in Ricerca 2013 grant No. RBFR13RQXM, and PRIN 20173LBZM2) for support.

Conflict of interest

The authors declare no conflict of interest.

Keywords: antimicrobial peptide · fully-developed helix · Langmuir-Blodgett technique · micrometric rods · molecular dynamics simulations

References

[1] G. Wang, *Antimicrobial Peptides: Discovery, Design and Novel Therapeutic Strategies*. Cab Intl, Wallingford, **2017**.

[2] P. Kumar, J. N. Kizhakkedathu, S.H. Straus, *Biomolecules*, **2018**, *8*, 4.

[3] D.I. Andersson, D. Hughes, *Drug Resistance Updates*, **2016**, *26*, 43-57.

[4] M. A. T. Blaskovich, *J. Med. Chem.*, **2016**, *59*, 10807-10836.

[5] The Peptaibol Database can be freely accessed at http://www.cryst.bbk.ac.uk/peptaibol.

[6] C. Toniolo, M. Crisma, F. Formaggio, C. Peggion, *Biopolymers*, **2001**, *60*, 396-419.

[7] M. Venanzi, E. Gatto, F. Formaggio, C. Toniolo, *J. Pept. Sci.*, **2017**, *23*, 104-116.

[8] C. Auvin-Guette, S. Rebuffat, Y. Prigent, B. Bodo, *J. Am. Chem. Soc.*, **1992**, *114*, 2170-2174.

[9] C. Toniolo, C. Peggion, M. Crisma, F. Formaggio, X. Shui, D. S. Eggleston, *Nat. Struct. Biol.*, **1994**, *1*, 908-914.

[10] M. Venanzi, E. Gatto, G. Bocchinfuso, A. Palleschi, L. Stella, C. Baldini, F. Formaggio, C. Toniolo, *J. Phys. Chem. B* **2006**, *110*, 22834-22841.

[11] M. Venanzi, E. Gatto, G. Bocchinfuso, A. Palleschi, L. Stella, F. Formaggio, C. Toniolo, *ChemBioChem* **2006**, *7*, 43-45.

[12] M. Venanzi, G. Bocchinfuso, E. Gatto, A. Palleschi, L. Stella, F. Formaggio, C. Toniolo, *ChemBioChem* **2009**, *10*, 91-97.

[13] G.M.L. Messina, M. De Zotti, R. Lettieri, E. Gatto, M. Venanzi, F. Formaggio, C. Toniolo, G. Marletta, *RSC Adv.*, **2016**, *6*, 46984-46993.

[14] C. Mazzuca, B. Orioni, M. Coletta, F. Formaggio, C. Toniolo, G. Maulucci, M. De Spirito, B. Pispisa, M. Venanzi, L. Stella, *Biophys. J.* **2010,** *99*, 1791-1800.

[15] C. Mazzuca, L. Stella, M. Venanzi, F. Formaggio, C. Toniolo, B. Pispisa, *Biophys. J.* **2005**, *88*, 3411-3421.

[16] L. Stella, C. Mazzuca, M. Venanzi, A. Palleschi, M. Didonè, F Formaggio, C. Toniolo, B. Pispisa, *Biophys. J.* **2004**, *86*, 936-945.

[17] N. Chaudhary, R. Nagaraj, *J. Coll. Interf. Sci.* **2011**, *360*, 139-147.

[18] K. Sankaranarayanan, A. Dhathathreyan, R. Miller, *J. Phys. Chem. B* **2010**, *114*, 8067-8075.

[19] R. Volinsky, S. Kolusheva, A. Berman, R. Jelinek, *Biochim. Biophys. Acta, Biomembr*. **2006**, *1758*, 1393-1407.

[20] B. Di Napoli, C. Mazzuca, P. Conflitti, M. Venanzi, A. Palleschi, *J. Phys. Chem. C* **2018**, *122*, 515-521.

[21] N. Kato, T. Sasaki, Y. Mukai, *Biochim. Biophys. Acta (Biomembr.)* **2015**, *1848*, 967-975.

[22] Z. Xu, J.W. Brauner, C.R. Flach, R. Mendelsohn, *Langmuir* **2004**, *20*, 3730-3733.

[23] C. Toniolo, A. Polese, F. Formaggio, M. Crisma, J. Kamphuis *J. Am. Chem. Soc.* **1996**, *118*, 2744-2745.

[24] a) C. Toniolo, M. Crisma, F. Formaggio, C. Peggion, V. Monaco, C. Goulard, S. Rebuffat, B. Bodo, *J.Am.Chem.Soc.* **1996**, *118*, 4952-4958; b) E. Locardi, S. Mammi, E. Peggion, V. Monaco, F. Formaggio, M. Crisma, C. Toniolo, B. Bodo, S. Rebuffat, J. Kamphuis, Q.B. Broxterman, *J. Pept. Sci.* **1998**, *4*, 389-399.

[25] K. Wüthrich in *NMR of Proteins and Nucleic Acids*, Wiley, New York, **1986**.

[26] C. Toniolo, *CRC Crit. Rev. Biochem.* **1980**, *9*, 1-44.

[27] E. Benedetti, A. Bavoso, B. Di Blasio, V. Pavone, C. Pedone, C. Toniolo, G.M. Bonora, *Biochem. Biophys. Res. Commun.* **1983**, *112*, 1056-1060.

[28] M. Crisma, F. Formaggio, A. Moretto, C. Toniolo, *Biopolymers* **2006**, *84*, 3-12.

[29] I.L. Karle *Folding, Aggregation and Molecular Recognition in Peptides. Acta Crystallogr. B* **1992**, *48*, 341-356.

[30] M. Lepère, C. Chevallard, J.-F. Hernandez, A. Mitraki, P. Guenoun, *Langmuir* **2007**, *23*, 8150-8155.

[31] T. Miyoshi, S. Kato *Langmuir* **2015**, 31, 9086-9096.

[32] D.F. Kennedy, M. Crisma, C. Toniolo, D. Chapman, *Biochemistry* **1991**, *30*, 6541-6548.

[33] M. Caruso, E. Placidi, E. Gatto, C. Mazzuca, L. Stella, G. Bocchinfuso, A. Palleschi, F. Formaggio, C. Toniolo, M. Venanzi *J. Phys. Chem. B* **2013**, *117*, 5448-5459.

[34] M. Caruso, E. Gatto, E. Placidi, G. Ballano, F. Formaggio, C. Toniolo, D. Zanuy, C. Aleman, M. Venanzi *Soft Matter* **2014**, *10*, 2508-2519.

[35] M. De Zotti, B. Biondi, C. Peggion, F. Formaggio, Y. Park, K.-S. Hahm, C. Toniolo, *Org. Biomol. Chem*. **2012**, *10*, 1285-1299.

[36] S. Pronk, S. Pall, R. Schulz, P. Larsson, P. Bjelkmar, R. Apostolov, M.R. Shirts, J.C. Smith, P.M. Kasson, D. van der Spoel, B. Hess, E. Lindahl, *Bioinformatics* **2013**, *29*, 845-854.

[37] C. Oostenbrink, A. Villa, A.E. Mark, W.F. van Gunsteren, *J. Comput. Chem.* **2004**, *25*, 1656-1676.

[38] H.J. Berendsen, J.V. Postma, W.F. van Gunsteren, A. Di Nola, J.R. Haak, *J. Chem. Phys.* **1984**, *81*, 3684-3690.

[39] W. Humphrey, A. Dalke, K. Schulten, *J. Mol. Graphics* **1996**, *14*, 33-38.

Controlling the Formation of Antimicrobial Peptide Films: Fully-Developed Helical Peptides Are Required to Obtain a Homogenous Coating over a Large Area

Marta De Zotti, Gabriele Corvi, Emanuela Gatto, Benedetta Di Napoli, Claudia Mazzuca, Antonio Palleschi, Ernesto Placidi, Barbara Biondi, Marco Crisma, Fernando Formaggio, Claudio Toniolo, and Mariano Venanzi*

Table of Content Graphics